Hemodynamic Modeling of Surgically Repaired Coarctation of the Aorta

LAURA J. OLIVIERI,[1] DIANE A. DE ZÉLICOURT,[2] CHRISTOPHER M. HAGGERTY,[2] KANISHKA RATNAYAKA,[1] RUSSELL R. CROSS,[1] and AJIT P. YOGANATHAN[2]

[1]Division of Cardiology, Children's National Medical Center, West Wing, W3-200, 111 Michigan Avenue, Washington, DC 20010, USA; and [2]Wallace H. Coulter Department of Biomedical Engineering, Georgia Institute of Technology, Atlanta, GA, USA

Associate Editor Pedro del Nido oversaw the review of this article.

Abstract—Late morbidity of surgically repaired coarctation of the aorta includes early cardiovascular and cerebrovascular disease, shortened life expectancy, abnormal vasomodulator response, hypertension and exercise-induced hypertension in the absence of recurrent coarctation. Observational studies have linked patterns of arch remodeling (Gothic, Crenel, and Romanesque) to late morbidity, with Gothic arches having the highest incidence. We evaluated flow in native and surgically repaired aortic arches to correlate respective hemodynamic indices with incidence of late morbidity. Three dimensional reconstructions of each remodeled arch were created from an anatomic stack of magnetic resonance (MR) images. A structured mesh core with a boundary layer was generated. Computational fluid dynamic (CFD) analysis was performed assuming peak flow conditions with a uniform velocity profile and unsteady turbulent flow. Wall shear stress (WSS), pressure and velocity data were extracted. The region of maximum WSS was located in the mid-transverse arch for the Crenel, Romanesque and Native arches. Peak WSS was located in the isthmus of the Gothic model. Variations in descending aorta flow patterns were also observed among the models. The location of peak WSS is a primary difference among the models tested, and may have clinical relevance. Specifically, the Gothic arch had a unique location of peak WSS with flow disorganization in the descending aorta. Our results suggest that varied patterns and locations of WSS resulting from abnormal arch remodeling may exhibit a primary effect on clinical vascular dysfunction.

Keywords—Aorta, Coarctation, Congenital heart disease, Magnetic resonance imaging, Wall shear stress.

Address correspondence to Laura J. Olivieri, Division of Cardiology, Children's National Medical Center, West Wing, W3-200, 111 Michigan Avenue, Washington, DC 20010, USA. Electronic mail: lolivier@cnmc.org

INTRODUCTION

Coarctation of the aorta is a common congenital cardiac defect, occurring in 6–8% of all congenital heart disease.[1] There is a wide spectrum of clinical severity to this disease. Typically, surgical management of coarctation of the aorta is necessary for patients that present during the newborn period with signs and symptoms of inadequate systemic perfusion from obstruction at the aortic isthmus. There are a variety of surgical approaches to correct coarctation of the aorta, the goal of each being to effectively restore systemic blood flow and eliminate the pressure drop across the aortic arch.

As these patients age, their repaired aortic arches grow and remodel. Late morbidity following successful coarctation repair is well-documented and includes early cardiovascular and cerebrovascular disease, coronary artery disease and shortened life expectancy.[1–3] Additionally, patients can commonly develop hypertension, exercise-induced hypertension and general vascular dysfunction.[4–6] There is a subset of patients that develop this late morbidity but do not have evidence of recurrent coarctation of the aorta, i.e. who do not have a significant arm-leg blood pressure difference (defined as the difference in systolic cuff pressures taken in the arm and leg, ideally simultaneously), and do not have a visible reduction in the aortic diameter by imaging or angiography.[7–9] One study indicates that this may encompass as many as 12% of patients who underwent coarctation repair and as many as 28% of patients who underwent repair beyond the age of 1 year.[10] They are a challenging group to manage as there is no lesion to intervene on based on standard imaging and diagnostic testing and clinical outcomes are difficult to predict. They are the focus of this study.

Using cardiac magnetic resonance imaging (MRI), Ou *et al.*[11] observed abnormal vascular responses in these patients with successfully repaired coarctation of the aorta correlated with abnormal aortic arch remodeling patterns in late follow-up of surgical repair. They created a classification scheme based on geometric criteria obtained from MR images comparing the width, W (defined as the transverse distance between the midpoints—or vessel centers—of the ascending to descending aorta), to the height, H (defined as the vertical distance from W to the highest vessel center of the aortic arch). It was postulated that these patients fit into one of three groups of arch morphology, which they termed Gothic, Crenel and Romanesque based on the ratio of H to W. This terminology was based on similarities between abnormal aortic arch remodeling patterns and these architectural styles (Figs. 1a, 1b, 1c). Using this classification scheme, they noted that patients with Gothic arches had a significantly higher incidence of vascular dysfunction when compared to the Romanesque group and to normal controls.[12] These patients do not exhibit any diagnosable re-coarctation; rather, they appear to have abnormal vasculature in the setting of successfully repaired coarctation. Why Romanesque arches have superior clinical outcomes as compared to the Gothic and Crenel groups remains unexplained. Given the drastic differences in underlying geometries, one possible explanation is the variation of the hemodynamics through these arches.

Previous studies have shown that, if carefully used and well-resolved, Computational Fluid Dynamics (CFD) can be an accurate method of predicting *in vitro* and *in vivo* hemodynamics.[13–16] Combined CFD and MRI studies of the staged surgical palliation (Fontan) for patients with single ventricle heart diseases have illustrated the importance of local hemodynamics on clinical outcome, and led to several technical suggestions and improvements.[17–19] Of particular relevance to our work, CFD has been applied to resolve the flow dynamics of patient specific aortas,[14,15] as well as to characterize the flow patterns and wall shear stresses (WSS) in coronary artery bypass grafts (CABG) and aneurysm development.[16] More recently, vendor-specific MRI tools to measure "four dimensional flow" have also been utilized to evaluate blood flow and calculate indices such as WSS in a real-time manner,[20,21] although with lower accuracy than CFD models.

Accordingly, our aim in this study is to use CFD, based on MRI-derived anatomical data, to simulate flow patterns in these remodeled arches. We hypothesize that differences among groups, which result in global performance differences, can be traced to differences at the level of the local hemodynamics, such as the WSS imposed on the aortic vessel walls. In order to narrow the number of variables and ease the identification of the relevant hemodynamic patterns and metrics, we focus our analysis on peak systole. Through this pilot study we hope to provide possible explanations for the variable incidence of vascular dysfunction seen among these patients and offer a method for detecting these abnormal hemodynamics.

METHODS

Subject Identification

After obtaining IRB approval, a retrospective ICD-9 directed search for "Coarctation of the Aorta" was performed in an outpatient hospital database and cardiac catheterization laboratory database (Children's National Medical Center, Washington, D. C.). This identified all patients with this congenital cardiac lesion followed at our institution since 2002 ($n = 511$).
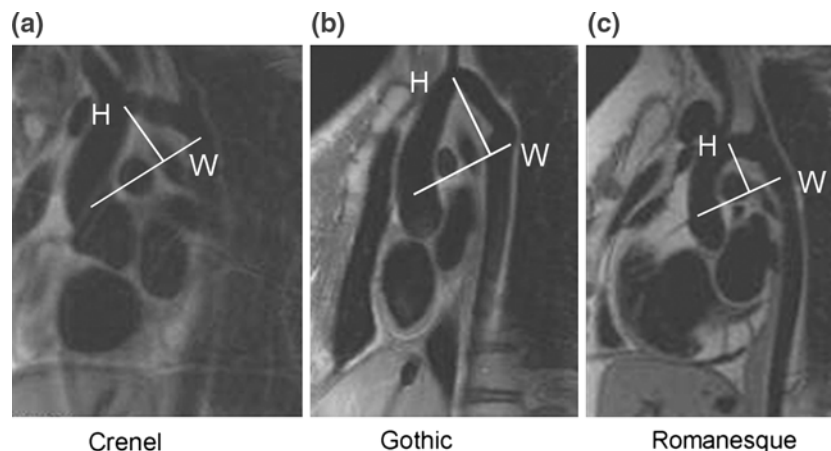

FIGURE 1. Arch types—three types of arches following surgical repair of coarctation of the aorta. Lines shown indicate the relationship of the height-to-width ratio of the thoracic aorta. H height, W width.

This cohort of patients was cross-matched with the cardiac MRI database to identify patients with coarctation of the aorta who had undergone a cardiac MRI at our institution ($n = 66$). Patients were included if they had a cardiac MRI performed following surgical repair of coarctation of the aorta ($n = 62$). Exclusion criteria included the presence of any other cardiac defect that would affect the development of the aorta (single ventricle, large ventricular septal defect, etc.), other left-sided cardiac abnormality, (aortic stenosis or mitral stenosis), presence of recurrent coarctation of the aorta and incomplete clinical records (27 patients). Of note, patients with bicuspid aortic valves without stenosis were not excluded. This search identified 35 appropriate subjects.

After a thorough examination of the cardiac MR images available for the 35 subjects retained, three patient datasets were selected for CFD analysis, which were considered to have the aortic geometries most representative of each one of the three remodeling categories (Crenel, Gothic, and Romanesque) according to previously published methods.[11] One additional dataset without pathology was retained as a normal comparison, which will be referred to as the Native arch.

MRI Data

All 35 patients retained for the clinical analysis underwent an MRI examination on a 1.5T scanner (GE, Milwaukee, WI) using a protocol that included cine steady state free precession (SSFP) imaging sequences with respiratory compensation and ECG gating. Due to the retrospective nature of data collection, various TE (1.48–1.63 ms) and TR (3.31–3.69 ms) were used in each imaging study to optimize the image in each case. A slice thickness of 10 mm and a field of view of 45 mm were used in all cases. Although preferred for validation of inlet modeling conditions, phase contrast data were not available from these retrospective datasets.

Three-Dimensional Aorta Reconstruction

Patient-specific aortic models of the four patients retained for the CFD investigation were reconstructed from the 2D stack of SSFP images. First, adaptive control grid interpolation was used between each slice to obtain approximately isotropic voxel sizes.[22] The region of interest was then segmented from each slice, using an in-house scaffolded shape-element algorithm,[23] such that the entire aorta from diaphragm through the first 5 mm of the head and neck vessels was reconstructed. A 3D level set-based surface evolution was run on the stack of segmented images to extract a set of smooth, coherent surface points. Finally, Geomagic Studio (Geomagic, Research Triangle Park, NC) was used to fit the point cloud with a smooth 3D surface.

Grid Construction

Each of the arch reconstructions was meshed according to a tetrahedral, hexcore meshing scheme using the Gambit software package (Fluent, Inc, Lebanon, NH). Two centimeter vessel extensions were added to the ascending aorta and to each head vessel to allow partial flow development in the inlet and to avoid backflow at the outlets. An appropriately sized boundary layer (0.1 mm height, growth factor of 1.2 and four layers) was added to each model to capture flow perturbations at the aortic wall. A hexcore mesh was used for the core of the blood volume, whose minimum cell dimensions created internal continuity with the prescribed boundary layer, with a maximum size limit of 1 mm. The final models had 296577, 525868, 126197 and 431649 elements in the Gothic, Crenel, Romanesque and Native arch models, respectively. Measures of mesh quality, including skewness and size, were within acceptable limits ensuring a high quality mesh. Furthermore, a recent analysis of grid sensitivity for modeling flow in the pediatric aorta using CFD demonstrated little variation in hemodynamic results despite varying the number of grid elements from 100,00 to 1,600,000.[24] Since the meshes generated for the present study all fall within this range, they are assumed to be sufficiently dense.

Flow Modeling

Flow through the aorta was simulated by mathematically discretizing the Navier–Stokes equations in each of the polygonal elements using FLUENT (Fluent, Inc, Lebanon, NH). Turbulent flow was approximated using the standard kappa-omega turbulence model.[25] The vessel walls were considered as rigid, no-slip surfaces for the purposes of this model. Blood was considered to be an incompressible, Newtonian fluid with a kinematic viscosity of 3.7 cSt and a density of 1060 kg/m^3. An unsteady pressure-based solver with second-order implicit time advancement scheme was selected using PISO (pressure-implicit with splitting of operators) for the pressure–velocity coupling algorithm, and PRESTO (pressure staggering option) for the pressure interpolation. Simulations were considered to be converged when the residuals of the continuity and momentum equations were reduced to 10^{-4}. In addition, pressure monitors were placed in the descending aorta to assess the solution convergence.

The constant, steady flow boundary conditions were set to represent peak systole because it has the highest flow rate and therefore the highest potential values of

WSS. A peak systolic velocity of 0.75 m/s and the percentages of flow exiting through each head and neck artery and the descending aorta (see Fig. 2) were taken from previously published and validated data.[26] The simulations were initialized by first performing laminar simulations with a flat inlet velocity profile, and progressively increasing the inflow rate until the mean inlet velocity reached 0.75 m/s. The converged laminar solution was then used as the initial condition for the turbulent simulations conducted using the same constant inlet velocity profile. Once the flow solution converged for each model, results were analyzed using Tecplot 360 (Tecplot, Bellevue, WA).

In evaluating blood flow through vessels, the WSS has been shown both *in vitro* and *in vivo* to affect vessel reactivity and protein expression on the endothelial cell surface.[27] Here, we examined each remodeled arch type as well as a native arch, paying particular interest to the WSS (τ_{wall}) levels. In general terms, WSS of flow through a cylindrical tube is determined by

$$\text{WSS} = \tau_{wall} = \lim_{r \to R} \mu \frac{\partial V}{\partial r}$$

where R is the vessel radius, ∂r is the differential radial position, V is the streamwise velocity, and μ is the dynamic viscosity. In this study, the WSS values were calculated with a FLUENT built-in function, using the streamwise and circumferential velocity gradients defined with respect to the inward normal vector to each surface element.

RESULTS

The values of WSS, peak velocity and the Reynolds numbers obtained for each of the four models can be found in Table 1. Figure 2 depicts the flow structures and velocity magnitudes observed in each of the four models using 3D streamtraces color-coded by the velocity magnitude normalized to the peak velocity to allow for an easier comparison across the four arches. Figure 3 is a closer depiction of the 3D streamtraces in the Native arch illustrating the Dean vortices that were observed in that particular model. Finally, values of WSS were calculated for each of the three remodeled arches and the native arch. Results are shown in Fig. 4 from the anterior-posterior view and in Fig. 5 from the cranial-caudal view.

To effectively compare the hemodynamics of the remodeled arches, a detailed description of the normal arch will first be presented. Subsequently, the remodeled
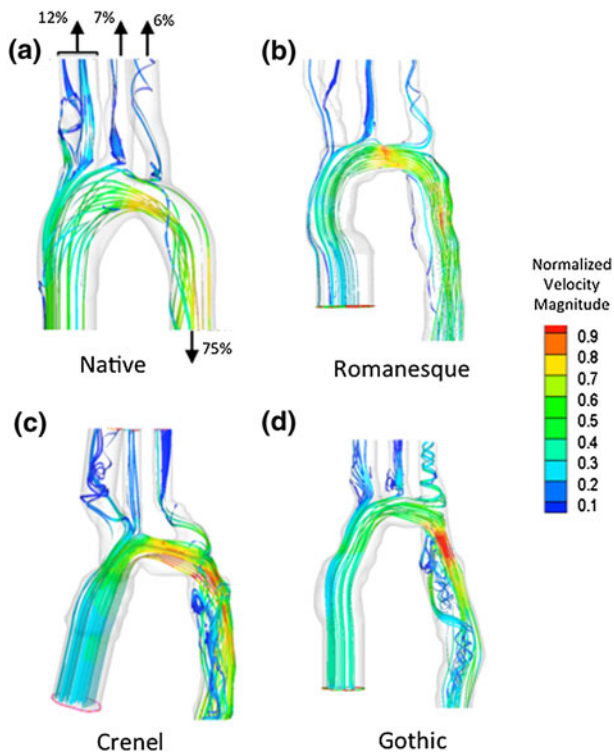

FIGURE 2. Three dimensional flow structures in each arch type—each arch is shown with flow structures encoded with velocity magnitude indexed in each case to peak velocity. Head vessel flow splits assumptions are also indicated. Peak velocities are seen in red.

TABLE 1. Results of WSS, velocity and Reynolds number for each arch type.

Arch type	Peak WSS (dyn/cm^2)	Peak velocity (m/s)	Reynolds number	Inlet diameter (mm)
Native	55	1.4	6385	20.6
Romanesque	144	3.0	4175	31.5
Crenel	166	2.7	4094	20.2
Gothic	120	2.5	4013	19.8

The Reynolds number is defined as UD/v, where $U = 0.75$ m/s is the mean velocity at the aortic inlet, $D = (\text{area}/\pi)^{1/2}$ is the equivalent diameter of the aortic inlet, and $v = 3.7$ cSt is the viscosity of blood.
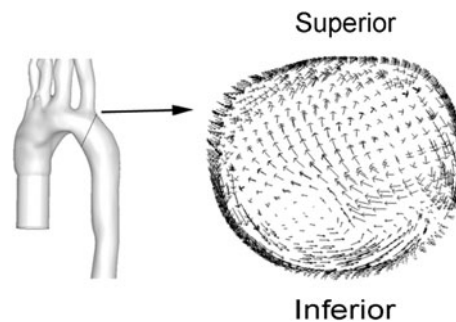

FIGURE 3. Three dimensional flow structures in the native arch demonstrating the counter-rotating Dean vortices in the ascending and descending native aorta.
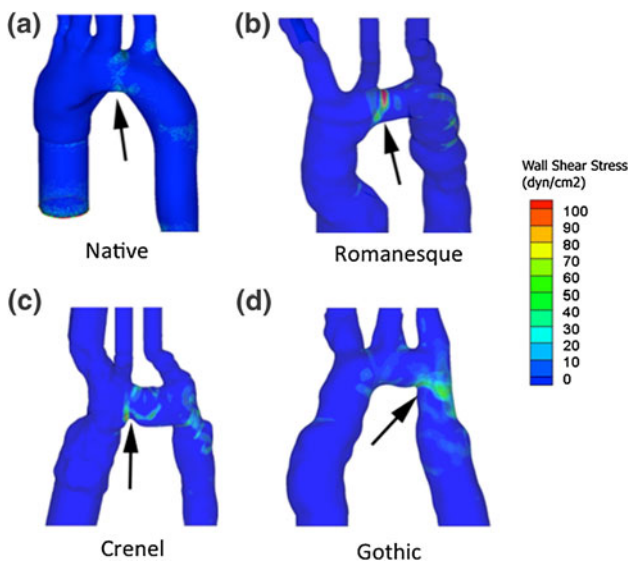
FIGURE 4. WSS magnitude of each arch type shown in the anterior–posterior view. Arrows indicate the area of peak WSS as indicated in red.
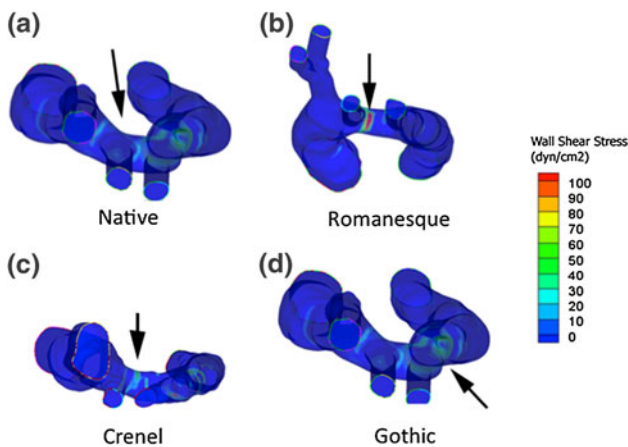

FIGURE 5. WSS magnitude of each arch type shown in the cranial-caudal view. Arrows indicate the area of peak WSS as indicated in red.

arches will be discussed, focusing on the altered characteristics.

Hemodynamics of the Native Aorta

The anatomy of the normal aortic arch (Fig. 2a) is characterized by a complex bending in three directions through the upper thorax: anterior-to-posterior, right-to-left, and of course superior-to-inferior. As a result of this bending, flow through the aorta has a significant amount of secondary flow structures that develop along its course; however, the smoothly curved profile of the aorta ensures that this hemodynamic complexity occurs with minimal inefficiency. This is realized by the

formation of the well-documented Dean vortices (Fig. 3), or two counter-rotating secondary flow structures, which counteract the outward angular momentum of blood flow through the aortic curvature by smoothly recirculating to the inner bend.[28] As a result, as seen in the Native arch (Fig. 2a), the bulk flow remains organized even at peak flow conditions, and there is only a slight flow separation observed after the isthmus. All streamlines appear in shades of green testifying for the fact that peak velocities remain close to the mean flow values. Convective flow acceleration (light orange streamlines in Fig. 2a) occurred through the mid-transverse arch as the aorta narrowed with peak velocities observed in the distal arch just beyond the takeoff of the left subclavian artery. Peak WSS values were also observed in the mid-transverse arch (Figs. 4a, 5a), as a result of the combined effects of vessel narrowing (leading to higher average velocities) and vessel curvature (skewing the peak velocities toward the outer bend of the arch).

Modeling the Post-Surgical Aortas

All three of the post-surgical aortas modeled in this study displayed characteristics closer to 'corners', rather than a smoothly-varying arch, particularly at the inner curvature. As a result, the characteristic behavior of the Dean vortices is not as apparent from the velocity streamtraces (Figs. 2b, 2d). The geometric irregularities lead to flow separation at the 'corners', which is associated with flow acceleration and high WSS along the outer vessel wall immediately downstream of the 'corner', and slow recirculating flow and varying WSS along the opposite inner wall. These characteristics are more pronounced as we progress from the Romanesque to the Crenel and Gothic arches.

It is interesting to note that, while the magnitudes of the peak WSS and velocities do not significantly differ across the three different types of arch remodeling (Table 1), their location, on the other hand, clearly varies. In the Romanesque and Crenel arches, flow acceleration and highest WSS occur within the transverse arch. In Gothic arches on the other hand, the height to width ratio is such that the transverse arch is almost non-existent. As a result, the flow acceleration and peak WSS occur along the outer wall, just downstream of the aortic isthmus (Figs. 2d, 4d). The sudden curvature is also associated with a large recirculation area along the inner wall downstream of the isthmus, and the flow is seen to destabilize deep into the descending aorta. It is worth noting that this trend is similar to what is present in unrepaired coarctation of the aorta, with peak, turbulent flow through the stenotic aortic isthmus.

DISCUSSION

Following surgical repair of coarctation of the aorta, a subset of patients, without clinical evidence of a recurrent coarctation, will develop late significant morbidity including early cardiovascular and cerebrovascular disease, shortened life expectancy, hypertension, and abnormal vascular reactivity. This patient population presents significant management challenges and is the focus of this study.

Physicians experienced in caring for these patients have noted that there are distinct arch shapes that are observed following surgery for coarctation of the aorta; named Crenel, Gothic and Romanesque. Whether these geometries are pre-existing and unique to the patient or whether they develop from remodeling changes from surgery is difficult to prove.[29] Our clinical results indicate that the shape of the aortic arch following surgical repair of coarctation of the aorta is not influenced by the type of surgical repair in our small series. This echoes what has been previously published in this regard.[12] Nevertheless, the shape of the remodeled arch has been noted to correlate with clinical status. Patients with Gothic-type remodeled arches have a higher incidence of late morbidity,[7] leading one to postulate that the shape of the arch could influence the hemodynamics in such a way to create pathologic flow, even in the absence of a recurrent coarctation. This was studied extensively by Ou et al.[30] who found an increased systolic wave reflection in the ascending aorta in Gothic arches, and correlated this finding with hypertension.

Numerous studies exist noting the effects of high WSS on endothelium, altering protein expression of the endothelial cell wall, which affects vessel distensibility and compliance.[31] Abnormal vessel compliance can result in pathologic states, the most common of which is the association between hypertension and atherosclerosis. Likewise, regions of low and oscillatory WSS have been implicated in disease progression.[32] Thus, both of these adverse environments must be considered when seeking a link between local hemodynamics and disease.

Our results clearly demonstrate differences in the local hemodynamic environment of post-surgical aortic arches compared to normal as a function of their geometry. All three remodeled arches yielded significantly higher peak WSS (ranging between 120 and 170 dyn/cm^2) than is seen in the native arch (55 dyn/cm^2). The location of the peak WSS in the three remodeled arches are systematically located directly downstream of the geometrical irregularities, or "corners", as these present obstacles that create a flow separation, with convective flow acceleration and high WSS along the outer bend of the aorta and slow flow recirculation along the inner wall. It is noteworthy that, despite apparently altered geometries, these flow disruptions and peak WSS occur in the transverse aortic arch in both Romanesque and Crenel arches, in a location similar to that of peak WSS in Native arches. In Gothic arches, on the other hand, peak WSS are recorded downstream of the aortic isthmus, rather than in the almost non-existent transverse aortic segment. Although there is no measurable constriction of the aorta, the sharp angulation between the ascending and descending aorta appears to have an effect similar to what is seen in unrepaired coarctation of the aorta, with peak, turbulent flow through the stenotic aortic isthmus. As such, the notable difference between the three remodeling types may not so much be due to the magnitude of the WSS (which were of the same order) than from their location.

At this point, it is important to recall that this pilot study solely focuses on the hemodynamics at peak systole. However, because of the sharpness and dimensions of these "corners", their impact on the local hemodynamics might be expected to hold throughout systole. Accordingly, we hypothesize that the regions of peak WSS reported herein might experience high WSS throughout systole. Additionally, the observed regions of flow separation may well be the site of oscillating WSS patterns once the time-varying flow profile is taken into consideration. The results reported herein would suggest an adjacent localization of high WSS and low, oscillatory WSS regions within the remodeled aortic arches, which can add even greater complexity to the response of the local endothelium. Previously published clinical findings have shown that patients with Gothic arches have a higher incidence of late morbidity following surgical repair despite normal global hemodynamic measures. From a clinical standpoint, this implies that global hemodynamic measures (such as arm-leg pressure difference or presence of brachial-femoral delay) may not be the appropriate means to fully assess the risk factors for morbidity in this patient population. Rather, the local hemodynamics, in particular the patterns of WSS along the length of the arch, should be assessed carefully.

There are limitations to the work presented in this paper. First, this is a pilot project where four arches were examined for their hemodynamics. Further investigation of the observed relationship between WSS magnitude/location and clinical morbidity would require modeling more arches of each morphology to confirm the existence of a causal relationship. Second, each of the models was built using retrospectively gathered two-dimensional imaging data with a slice thickness of 10 mm, which can cause significant artifact when attempting to build a 3D reconstruction and creating a mesh with elements in the 1–2 mm size

range. Unfortunately, phase contrast data was not available to validate the flow conditions used in the modeling, which would have been optimal. Third, each of the models used an assumed uniform velocity profile at the inlet and assumed a normal outflow distribution through the head vessels and descending aorta at peak systole, which only represents one time-point in the cardiac cycle. Additionally, there are several assumptions inherent in modeling, such as rigid walls, modeling of turbulent flow and modeling viscous fluids, which each have their own sources of inherent error. Finally, the time at which the distinct arch types develop is not clear; therefore, additional pre-procedure analysis and short-term post-procedure analysis are needed to determine if these findings are innate to the patients themselves or to a post-surgical remodeling process. Despite these limitations, the overall trend observed in this pilot study is that there are important differences in all hemodynamic properties of the Gothic arch when compared to each of the other arches. The impact of variation of flow rates, grid sensitivity and the use of prospectively acquired image and velocity data may alter the values of WSS and velocity gradients among the arches, but would not be expected to alter the relationship of these data between the arches as they are all subject to identical limitations. Further, and most importantly, the location of maximum WSS, flow disruption and flow acceleration would not be affected.

Future studies will seek to incorporate patient-specific flow conditions to more accurately assess *in vivo* stress states, particularly because some of the late morbidity includes vascular dysfunction that is apparent in high-output states, such as exercise. Real-time four-dimensional flow using MRI acquired data would be one possible method to accomplish this.

CONCLUSIONS

This study presents the hemodynamics of various shaped aortic arches following surgical repair, in an effort to better understand why certain aortic arch shapes (namely Gothic arches) are associated with higher morbidity than others. All post-surgical arches were observed to yield higher flow disturbances and elevated peak WSS compared to the Native configuration. More importantly, the Gothic arch had a unique location of peak WSS, in the descending aorta immediately downstream of the aortic isthmus), whereas these were found in the transverse aorta in all other arch types. These results suggest that the location of peak WSS may be an important contributor to clinical vascular dysfunction.

REFERENCES

[1] Cohen, M., V. Fuster, P. M. Steele, D. Driscoll, and D. C. McGoon. Coarctation of the aorta. Long-term follow-up and prediction of outcome after surgical correction. *Circulation* 80:840–845, 1989.

[2] Puranik, R., V. T. Tsang, S. Puranik, et al. Late magnetic resonance surveillance of repaired coarctation of the aorta. *Eur. J. Cardiothorac. Surg.* 36:91–95, 2009 (discussion 95).

[3] Warnes, C. A., R. G. Williams, T. M. Bashore, et al. ACC/AHA 2008 guidelines for the management of adults with congenital heart disease: a report of the American College of Cardiology/American Heart Association Task Force on Practice Guidelines (Writing Committee to Develop Guidelines on the Management of Adults With Congenital Heart Disease). Developed in Collaboration With the American Society of Echocardiography, Heart Rhythm Society, International Society for Adult Congenital Heart Disease, Society for Cardiovascular Angiography and Interventions, and Society of Thoracic Surgeons. *J. Am. Coll. Cardiol.* 52:e1–e121, 2008.

[4] de Divitiis, M., C. Pilla, M. Kattenhorn, et al. Vascular dysfunction after repair of coarctation of the aorta: impact of early surgery. *Circulation* 104:I165–I170, 2001.

[5] Mack, G., G. H. Burch, and D. J. Sahn. Coarctation of the aorta. *Curr. Treat. Options Cardiovasc. Med.* 1:347–354, 1999.

[6] Webb, G. Treatment of coarctation and late complications in the adult. *Semin. Thorac. Cardiovasc. Surg.* 17:139–142, 2005.

[7] Ou, P., E. Mousseaux, D. S. Celermajer, et al. Aortic arch shape deformation after coarctation surgery: effect on blood pressure response. *J. Thorac. Cardiovasc. Surg.* 132:1105–1111, 2006.

[8] Hoimyr, H., T. D. Christensen, K. Emmertsen, et al. Surgical repair of coarctation of the aorta: up to 40 years of follow-up. *Eur. J. Cardiothorac. Surg.* 30:910–916, 2006.

[9] Hager, A., S. Kanz, H. Kaemmerer, C. Schreiber, and J. Hess. Coarctation Long-term Assessment (COALA): significance of arterial hypertension in a cohort of 404 patients up to 27 years after surgical repair of isolated coarctation of the aorta, even in the absence of restenosis and prosthetic material. *J. Thorac. Cardiovasc. Surg.* 134:738–745, 2007.

[10] Seirafi, P., K. Warner, R. L. Geggel, et al. Repair of coarctation of the aorta during infancy minimizes the risk of late hypertension. *Ann. Thorac. Surg.* 66:1378–1382, 1998.

[11] Ou, P., D. Bonnet, L. Auriacombe, et al. Late systemic hypertension and aortic arch geometry after successful repair of coarctation of the aorta. *Eur. Heart J.* 25:1853–1859, 2004.

[12] Ou, P., D. S. Celermajer, E. Mousseaux, et al. Vascular remodeling after "successful" repair of coarctation: impact of aortic arch geometry. *J. Am. Coll. Cardiol.* 49:883–890, 2007.

[13]Glor, F. P., J. J. Westenberg, J. Vierendeels, M. Danilouchkine, and P. Verdonck. Validation of the coupling of magnetic resonance imaging velocity measurements with computational fluid dynamics in a U bend. *Artif. Organs* 26:622–635, 2002.

[14]Leuprecht, A., K. Perktold, S. Kozerke, and P. Boesiger. Combined CFD and MRI study of blood flow in a human ascending aorta model. *Biorheology* 39:425–429, 2002.

[15]Wood, N. B., S. J. Weston, P. J. Kilner, A. D. Gosman, and D. N. Firmin. Combined MR imaging and CFD simulation of flow in the human descending aorta. *J. Magn. Reson. Imaging* 13:699–713, 2001.

[16]Frauenfelder, T., E. Boutsianis, T. Schertler, *et al.* Flow and wall shear stress in end-to-side and side-to-side anastomosis of venous coronary artery bypass grafts. *Biomed. Eng. Online* 6:35, 2007.

[17]Ensley, A. E., P. Lynch, G. P. Chatzimavroudis, C. Lucas, S. Sharma, and A. P. Yoganathan. Toward designing the optimal total cavopulmonary connection: an in vitro study. *Ann. Thorac. Surg.* 68:1384–1390, 1999.

[18]Soerensen, D. D., K. Pekkan, D. de Zelicourt, *et al.* Introduction of a new optimized total cavopulmonary connection. *Ann. Thorac. Surg.* 83:2182–2190, 2007.

[19]Pizarro, C., and M. R. De Leval. Surgical variations and flow dynamics in cavopulmonary connections: a historical review. *Semin. Thorac. Cardiovasc. Surg. Pediatr. Card Surg. Annu.* 1:53–60, 1998.

[20]Frydrychowicz, A., R. Arnold, D. Hirtler, *et al.* Multidirectional flow analysis by cardiovascular magnetic resonance in aneurysm development following repair of aortic coarctation. *J. Cardiovasc. Magn. Reson.* 10:30, 2008.

[21]Frydrychowicz, A., A. F. Stalder, M. F. Russe, *et al.* Three-dimensional analysis of segmental wall shear stress in the aorta by flow-sensitive four-dimensional-MRI. *J. Magn. Reson. Imaging* 30:77–84, 2009.

[22]Frakes, D. H., C. P. Conrad, T. M. Healy, *et al.* Application of an adaptive control grid interpolation technique to morphological vascular reconstruction. *IEEE Trans. Biomed. Eng.* 50:197–206, 2003.

[23]Frakes, D. H., M. J. Smith, J. Parks, S. Sharma, S. M. Fogel, and A. P. Yoganathan. New techniques for the reconstruction of complex vascular anatomies from MRI -images. *J. Cardiovasc. Magn. Reson.* 7:425–432, 2005.

[24]Yang, N., S. Deutsch, E. G. Paterson, and K. B. Manning. Hemodynamics of an end-to-side anastomotic graft for a pulsatile pediatric ventricular assist device. *J. Biomech. Eng.* 132:031009, 2010.

[25]DeGroff, C. G., R. Shandas, and L. Valdes-Cruz. Analysis of the effect of flow rate on the Doppler continuity equation for stenotic orifice area calculations: a numerical study. *Circulation* 97:1597–1605, 1998.

[26]Yull Park, J., C. Young Park, C. Mo Hwang, K. Sun, and B. Goo Min. Pseudo-organ boundary conditions applied to a computational fluid dynamics model of the human aorta. *Comput. Biol. Med.* 37:1063–1072, 2007.

[27]Barbee, K. A., T. Mundel, R. Lal, and P. F. Davies. Subcellular distribution of shear stress at the surface of flow-aligned and nonaligned endothelial monolayers. *Am. J. Physiol.* 268:H1765–H1772, 1995.

[28]Kilner, P. J., G. Z. Yang, R. H. Mohiaddin, D. N. Firmin, and D. B. Longmore. Helical and retrograde secondary flow patterns in the aortic arch studied by three-directional magnetic resonance velocity mapping. *Circulation* 88:2235–2247, 1993.

[29]Lashley, D., J. Curtin, P. Malcolm, A. Clark, and L. Freeman. Aortic arch morphology and late systemic hypertension following correction of coarctation of aorta. *Congenit. Heart Dis.* 2:410–415, 2007.

[30]Ou, P., D. Celermajer, and O. Raisky. Angular (Gothic) aortic arch leads to enhanced systolic wave reflection, central aortic stiffness, and increased left ventricular mass late after aortic coarctation repair: evaluation with magnetic resonance flow mapping. *J. Thorac. Cardiovasc. Surg.* 135:62–68, 2008.

[31]Davies, P. F., K. A. Barbee, R. Lal, A. Robotewskyj, and M. L. Griem. Hemodynamics and atherogenesis. Endothelial surface dynamics in flow signal transduction. *Ann. N. Y. Acad. Sci.* 748:86–102, 1995; (discussion 102–3).

[32]Davies, P. F., J. A. Spaan, and R. Krams. Shear stress biology of the endothelium. *Ann. Biomed. Eng.* 33:1714–1718, 2005.